



## Article

# A Portable Electrochemical Dopamine Detector Using a Fish Scale-Derived Graphitized Carbon-Modified Screen-Printed Carbon Electrode

Feng Yang <sup>1,2,†</sup>, Xiao Han <sup>1,†</sup>, Yijing Ai <sup>1</sup> , Bo Shao <sup>1</sup>, Weipin Ding <sup>2</sup>, Kai Tang <sup>2,\*</sup> and Wei Sun <sup>1,\*</sup> 

- <sup>1</sup> Hainan Engineering Research Center of Tropical Ocean Advanced Optoelectronic Functional Materials, Key Laboratory of Laser Technology and Optoelectronic Functional Materials of Hainan Province, Key Laboratory of Functional Materials and Photoelectrochemistry of Haikou, College of Chemistry and Chemical Engineering, Hainan Normal University, Haikou 571158, China; likeyangff@126.com (F.Y.); hanxiao0659@163.com (X.H.); aiyijing1995@163.com (Y.A.); m17264392385@163.com (B.S.)
- <sup>2</sup> Haikou Marine Geological Survey Center, China Geological Survey, Haikou 571127, China; gzsdingwp@126.com
- \* Correspondence: 18976530623@163.com (K.T.); sunwei@hainnu.edu.cn (W.S.)
- † These authors contributed equally to this work.

**Abstract:** In this paper, a highly conductive alkali-activated graphitized carbon (a-GC) was prepared using tilapia fish scales as precursors through enzymolysis, activation and pyrolytic carbonization methods. The prepared a-GC was modified on the surface of a screen-printed carbon electrode to construct a flexible portable electrochemical sensing platform, which was applied to the differential pulse voltametric detection of dopamine (DA) using a U-disk electrochemical workstation combined with a smart phone and Bluetooth. The prepared a-GC possesses good electrical conductivity, a large specific surface area and abundant active sites, which are beneficial for the electrooxidation of DA molecules and result in excellent sensitivity and high selectivity for DA analysis. Under the optimal conditions, the oxidation peak current of DA increased gradually, with its concentrations in the range from 1.0  $\mu\text{mol/L}$  to 1000.0  $\mu\text{mol/L}$ , with the detection limit as low as 0.25  $\mu\text{mol/L}$  (3S/N). The proposed sensor was further applied to the determination of DA in human sweat samples, with satisfactory results, which provided an opportunity for developing noninvasive early diagnosis and nursing equipment.

**Keywords:** electrochemical sensor; screen-printed carbon electrode; graphitized carbon; dopamine



**Citation:** Yang, F.; Han, X.; Ai, Y.; Shao, B.; Ding, W.; Tang, K.; Sun, W. A Portable Electrochemical Dopamine Detector Using a Fish Scale-Derived Graphitized Carbon-Modified Screen-Printed Carbon Electrode. *Molecules* **2024**, *29*, 744. <https://doi.org/10.3390/molecules29030744>

Academic Editors: Carlos Alemán, Mariana Emilia Ghica and Gianantonio Battistuzzi

Received: 7 December 2023  
Revised: 11 January 2024  
Accepted: 29 January 2024  
Published: 5 February 2024



**Copyright:** © 2024 by the authors. Licensee MDPI, Basel, Switzerland. This article is an open access article distributed under the terms and conditions of the Creative Commons Attribution (CC BY) license (<https://creativecommons.org/licenses/by/4.0/>).

## 1. Introduction

Dopamine (DA) is an important neurotransmitter present in the central nervous system of mammals and can affect behavior, emotion and health [1]. The changes in the DA concentration level in the human body will cause a series of diseases, such as Parkinson's disease, mental abnormality, senile dementia, and emotional disorders [2]. Therefore, the sensitive and accurate measurement of DA is crucial for the prevention and treatment of these diseases. DA can also be found in human sweat, which exhibits positive correlation with its content in blood [3]. Thus, the detection of DA in sweat sample can lead to a non-invasive analysis with real-time monitoring [4,5], which is convenient for disease diagnostics and health control. At present, different technologies, including colorimetric method [6], fluorescence method [7], and surface-enhanced Raman spectroscopy [8], have been used for DA analysis. However, these techniques are often time-consuming and involve expensive instruments, which limits their real-life applications. A focus of the current research is on developing a cost-effective method for the quantitative determination of DA with simple operation and on-site capability.

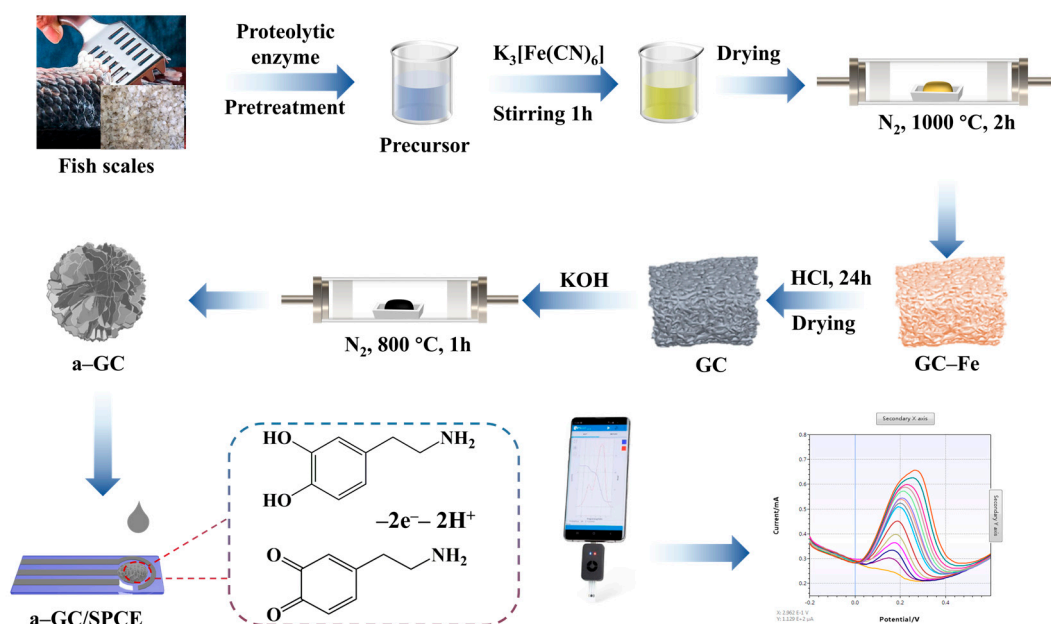
Electrochemical sensors have exhibited many advantages, such as high sensitivity, good selectivity and fast response [9]. However, the practical applications of traditional

solid electrodes have been limited due to the disadvantages, such as the larger size (diameter of 1–4 mm), complex operation and low repeatability (<20% relative standard deviation) [10]. The combination of a portable electrochemical sensor and a smart phone has been designed with various modifiers and practical applications. For example, Shao et al. [11] designed a portable electrochemical sensing platform with a screen-printed carbon electrode (SPCE) and a Bluetooth electrochemical workstation, which was suitable for the analysis of the indole-3-acetic acid concentration in various tissues of mung bean sprouts. Parrilla et al. [12] modified an SPCE with 1, 2-naphthoquinone-4 sulfonate to construct a sensor for the detection of amphetamine. Chen et al. [13] developed a wireless portable electrochemical sensor based on an SPCE to analyze the indole-3-acetic acid content in different parts of pea seedlings. Zhou et al. [14] developed a high-performance electrochemical sensor based on a reduced graphene oxide and carboxyl-functionalized multi-walled carbon nanotube hybrid-modified SPCE for simultaneous detection of cadmium ion and lead ion. Yamuna et al. [15] prepared a pyrochlore-type lanthanum tin oxide nanoparticle-modified SPCE for carbaryl detection with the limit of detection as 0.4 nmol/L. Nagles et al. [16] developed an ionic liquid-treated chitosan-single-walled carbon nanotube-modified SPCE for simultaneous detection of DA and uric acid (UA). The construction and application of these portable electrochemical sensors will enable the development of point-of-care devices for practical electrochemical applications.

So far, various nanomaterials, such as metal nanoparticles, metal oxides, carbon nanomaterials and conductive polymers [17–20], have been used for the oxidation of DA. Among them, carbon nanomaterials have attracted increasing attention due to the good conductivity (>500 S/m) [21] and adjustable physical/chemical properties. Biomass-derived carbon, a kind of renewable carbon materials obtained from animal and plant wastes, is widely used in electrochemical sensing applications because of the high specific surface area, rich porous structure, superior physical and chemical stability [22]. For example, Zhang et al. [23] constructed an electrochemical sensing platform based on a composite combination of Kiwi skin-derived carbon and zinc chloride nanoparticles, which was used to simultaneously detect ascorbic acid (AA), DA and UA, with the corresponding detection limits (S/N = 3) of 0.02  $\mu\text{M}$ , 0.16  $\mu\text{M}$ , and 0.11  $\mu\text{M}$ . Mahmood et al. [24] converted biomass-based film composed of kraft lignin and cellulose nanofibers into porous graphene and used it for the voltametric detection of DA, which demonstrated that biomass-based material had the potential to be transformed into carbon materials with good electrochemical performance. Padmapriya et al. [25] prepared a phosphorus and nitrogen dual-doped carbon quantum dot-modified electrode with the banana flower bract extract as a precursor and used it for DA detection in the ultralow detection limit (picomolar). Sha et al. [26] synthesized a shaddock peel-derived carbon nanoball aggregation network-based aerogel, which had a large surface area (446.39  $\text{m}^2/\text{g}$ ) and hierarchical meso-microporous structure, and may provide a favorable path for electrolyte penetration and transportation. The above reports indicate the great promise of biomass-derived carbon for the electroanalysis, and it remains to be studied to further improve the electroanalysis performance of sensors.

High-temperature pyrolysis, catalytic pyrolysis and alkali activation are commonly used methods to adjust the morphological structure and graphitization degree of biomass carbon [27–31]. The graphitization degree of biomass carbon affects the defect site density and conductivity [32]; thus, it is a good strategy to improve the electrochemical performance by adjusting the graphitization degree of biomass carbon. Cheng et al. [33] prepared a highly graphitized N-doped porous carbon material derived from biomass with ferric ammonium citrate as an active agent. He et al. [34] prepared microporous carbon with a large specific surface area (2208  $\text{m}^2/\text{g}$ ) and high conductivity (2.38 S/cm) by controlling the activation temperature of biomass pyrolysis with potassium ferrate as a catalyst and activation agent. Zhao et al. [35] prepared graphene-like nitrogen-doped carbon using chitosan as a precursor and ferric chloride as a soft template. Therefore, biomass-derived porous carbons with a high graphitization degree, large specific surface area and high conductivity are expected to achieve excellent sensing performance.

In this paper, alkali-activated graphitized carbon (a-GC) was prepared using fish scales as precursors via enzymolysis, activation and the two-step pyrolytic carbonization method, with  $K_3[Fe(CN)_6]$  as the catalyst. By employing an a-GC-modified SPCE as the base electrode, rapid and sensitive detection of DA was realized on the U-disk electrochemical workstation combined with a smart phone through Bluetooth. The preparation process for the a-GC and the application in portable electrochemical sensor are illustrated in Scheme 1, with the detailed procedures described in Section 3. The fish scales used in the experiment are tilapia scale wastes that are abundant in Hainan Province of China owing to its well-developed fishery industry, where low-value biomass waste is converted into high-value products in large-scale preparation through pyrolysis technology. As demonstrated below, graphitized carbon obtained via this process shows higher electrical conductivity, which is very promising both in the sensing platform as a modified electrode material and in other energy conversion and storage fields. The results in the paper provide some insights for the recycling of fish scales and the development of novel functional carbon materials from fishery waste.



**Scheme 1.** Synthesis of a-GC and electrochemical detection process for DA using a U-disk electrochemical workstation.

## 2. Results and Discussion

### 2.1. Characterizations of a-GC

The morphological features of a-GC produced via two-step carbonization were characterized by means of a field emission scanning electron microscope (FESEM) with the corresponding results obtained at  $10,000\times$ ,  $20,000\times$  and  $100,000\times$  magnifications shown in Figure 1A–C. The gradually enlarged SEM image indicates the prepared a-GC exhibited a flower-like structure with a diameter of  $\sim 5\ \mu\text{m}$ , which was formed by the staggered accumulation lamellas with a thickness of  $\sim 36\ \text{nm}$ . The flower-like structure of a-GC as an electrode material may greatly enhance the effective electrode area and facilitate the diffusion of analytes in the electrochemical processes. The scanning electron microscopic–energy dispersive X-ray spectroscopic results in Figure 1D show the presence of C, N, O and Fe in a-GC. Notably, the Fe content of 8.13 wt% might have originated from the incomplete removal of iron from the GC-Fe, which might enhance the electrocatalytic activity and affinity of a-GC through the chelation of Fe and DA [36]. Elemental mapping micrographs of C (Figure 1E), O (Figure 1F), Fe (Figure 1G) and N (Figure 1H) indicate that all the elements were uniformly distributed on the surface of the a-GC.

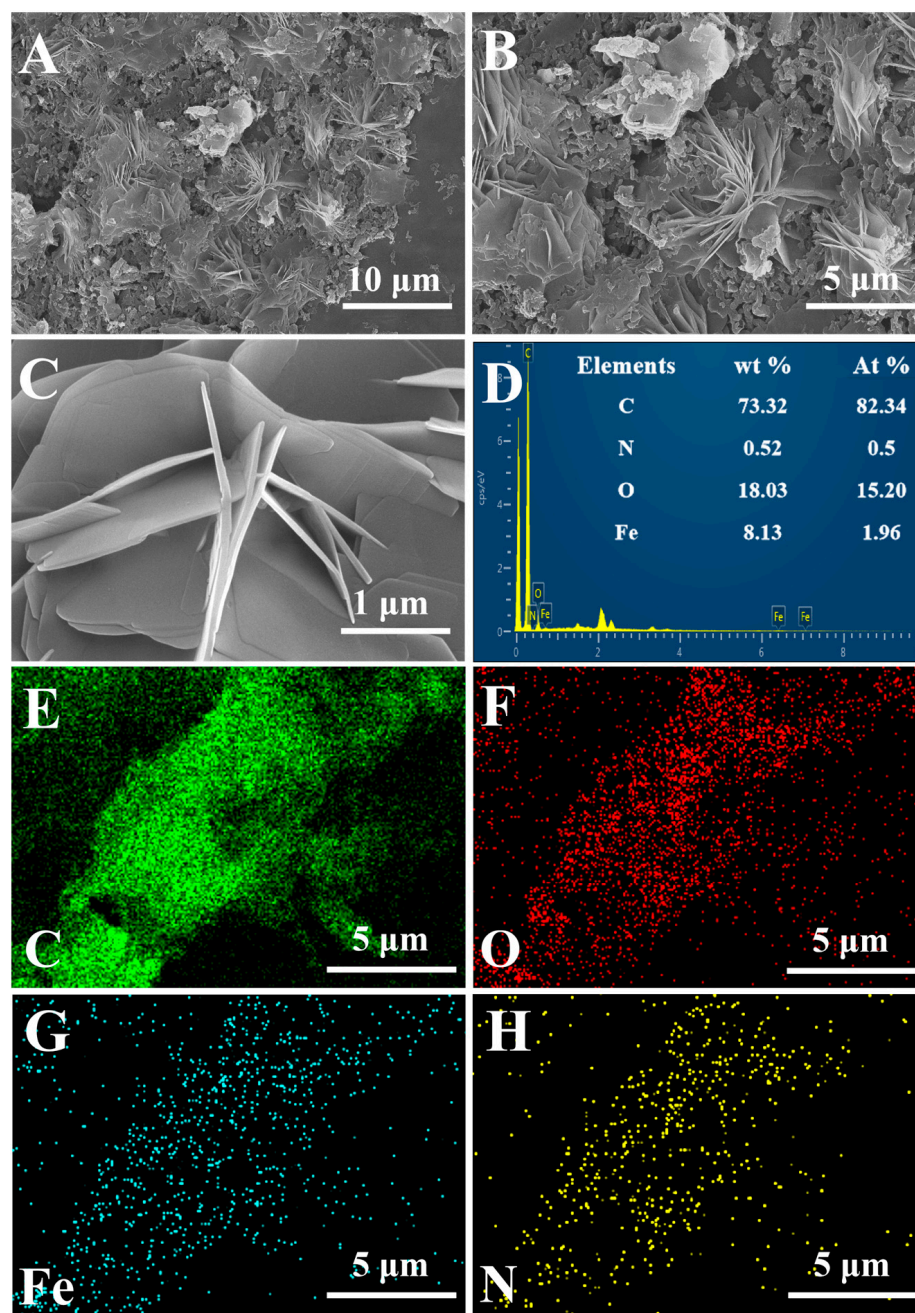


**Figure 1.** (A–C) Scanning electron microscopy images of a-GC at 10,000 $\times$ , 20,000 $\times$  and 100,000 $\times$  magnifications, (D) energy dispersive X-ray spectroscopy spectrogram of a-GC, elemental mapping of (E) C, (F) O, (G) Fe and (H) N of a-GC.

The morphological structures of a-GC at different magnifications were investigated using transmission electron microscopy (TEM) at 30,000 $\times$  and 100,000 $\times$  magnifications, with the results shown in Figure 2A,B. The a-GC displayed an obvious layered structure, which could increase the specific surface area and then provide more attachment points for further interaction with DA. The X-ray diffractometer (XRD) pattern of the a-GC (Figure 2C) showed a sharp peak at 26.42 $^{\circ}$  and a broad diffraction peak at 44.39 $^{\circ}$ , which corresponded to the (002) lattice plane and the (101) phase of graphitized carbon, confirming the existence of graphitized carbon obtained via a solid-state pyrolysis process [25].

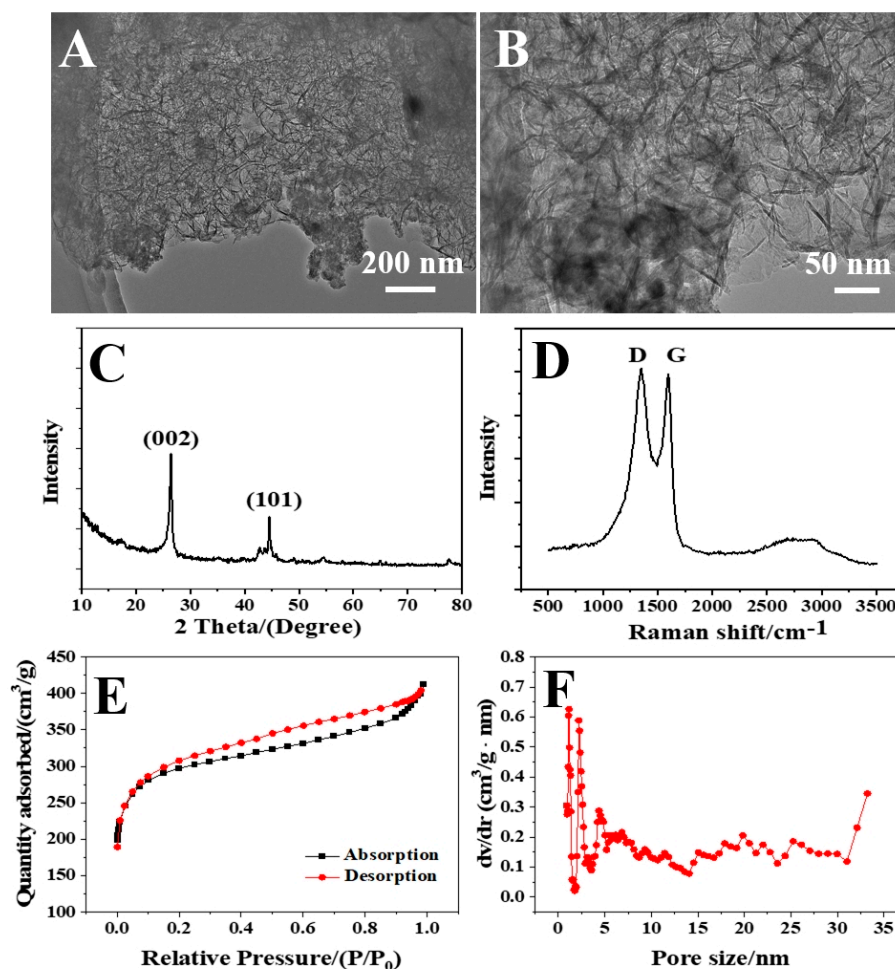


**Figure 2.** (A,B) Transmission electron microscopy images at 30,000 $\times$  and 100,000 $\times$  magnification, (C) XRD pattern, (D) Raman spectrum, (E) the N<sub>2</sub> adsorption and desorption isotherm and (F) the pore size distribution curve of a-GC.

The graphitic structure could be further verified via the Raman spectroscopic result (Figure 2D), in which the D and G peaks were located at 1350 cm<sup>-1</sup> and 1580 cm<sup>-1</sup>, with the intensity ratio ( $I_D/I_G$ ) as 1.02. Generally, it is believed that the D band originates from the defects of graphite and G band is thought to represent the degree of graphitization [37]. The  $I_D/I_G$  value indicated that the GC-a had a graphitization degree with some defects that may be ascribed to the N-doping. Therefore, fish scale-based biomass carbon with a high graphitization degree has been successfully synthesized using the two-step carbonization and KOH activation process.

The pore size distribution and surface area of the a-GC were further investigated via Brunauer–Emmett–Teller (BET) and N<sub>2</sub> adsorption–desorption measurements. As shown in Figure 2E, a-GC exhibited a type II isotherm and hysteresis loop in the relative equilibrium pressure ( $P/P_0$ ) range of 0–1.0, indicating a mainly microporous structure. In addition, the BET specific surface area of the a-GC was 1093.5 m<sup>2</sup>/g, with the major peak of pore size distributed in 1.1 nm and 2.2 nm (Figure 2F), which indicated that the a-GC possessed abundant micropores (<2.0 nm) and mesopores (from 2.0 to 50 nm). The presence of microporous will facilitate electron transfer and DA adsorption. Moreover, the mesopores offer a larger active area and good corridor structure for the adsorption of DA molecules, which may be beneficial to the diffusion of DA molecules on the surface of the modified electrode.

## 2.2. Electrochemical Properties of a-GC/SPCE

The electrochemical performances of working electrodes are often checked using the redox responses of  $[\text{Fe}(\text{CN})_6]^{3-}$ , which is a commonly used probe to evaluate the electrochemical properties of the modifier on the surface of a working electrode. Therefore, the electrochemical behaviors of 1.0 mmol/L  $[\text{Fe}(\text{CN})_6]^{3-}$  at an SPCE and an a-GC/SPCE in a 0.5 mol/L KCl-supporting electrolyte were studied via cyclic voltammetry (CV) at a scan rate of 0.1 V/s. As shown in curve a in Figure 3A, an oxidation peak of 29.46  $\mu\text{A}$  ( $I_{\text{pa}}$ ) at 0.25 V and a reduction peak of 27.68  $\mu\text{A}$  ( $I_{\text{pc}}$ ) at 0.11 V were observed. Meanwhile, on an a-GC/SPCE (curve b), the  $I_{\text{pa}}$  and  $I_{\text{pc}}$  increased to 44.65 mA and 48.64 mA, which could be ascribed to the active surface area and accelerated electron transfer rate of the a-GC on the electrode surface.

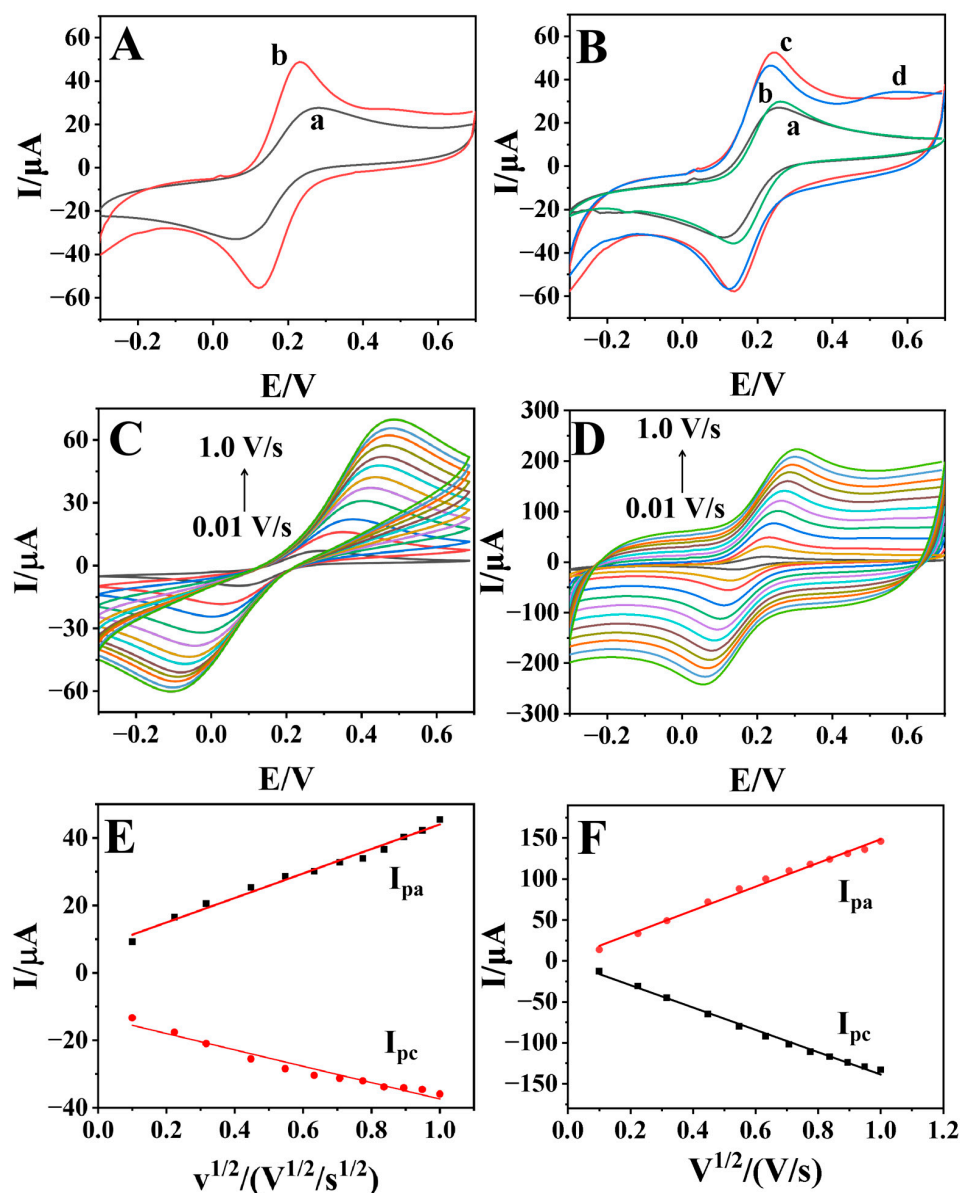


**Figure 3.** Cyclic voltammograms of (A) different modified electrodes (a: SPCE, b: a-GC/SPCE) and (B) different concentrations of a-GC modified on SPCE (a–d: 0.5, 1.0, 1.5, 2.0 mg/mL) in 1.0 mmol/L  $[\text{Fe}(\text{CN})_6]^{3-}$  and 0.5 mol/L KCl solution at a scan rate of 0.1 V/s; cyclic voltammograms of (C) SPCE and (D) a-GC/SPCE at different scan rates (0.01, 0.05, 0.1, 0.2, 0.3, 0.4, 0.5, 0.6, 0.7, 0.8, 0.9, 1.0 V/s) in 1.0 mmol/L  $[\text{Fe}(\text{CN})_6]^{3-}$  and 0.5 mol/L KCl solution, and the corresponding linear relationship between  $I_p$  and  $v^{1/2}$  of (E) SPCE and (F) a-GC/SPCE.

In order to optimize the quantity of a-GC immobilized on the electrode surface, CV curves of SPCE modified with an increasing concentration of a-GC suspension from 0.5, 1.0, 1.5 and 2.0 mg/mL were recorded in 1.0 mmol/L  $[\text{Fe}(\text{CN})_6]^{3-}$ . As shown in Figure 3B, the redox peak current increased from 27.04  $\mu\text{A}$  to 52.54  $\mu\text{A}$  as the concentration of the a-GC suspension increased from 0.5 mg/L to 1.5 mg/L. However, when the concentration was further increased to 2.0 mg/mL, the redox peak current was observed to decrease to 46.47  $\mu\text{A}$ , which may be due to the increase in the thickness of the a-GC film on the electrode surface. Also, the background peak increased on the a-GC/SPCE at a higher a-GC concentration, which could be ascribed to the increase in the thickness of the a-GC film with large double-layer charged current. As a result, 25  $\mu\text{L}$  1.5 mg/mL a-GC suspension was selected as the optimal quantity of modifier for the further electrochemical investigations.

To explore the electrochemical effective area of SPCE and a-GC/SPCE, CV curves were recorded in 1.0 mmol/L  $[\text{Fe}(\text{CN})_6]^{3-}$  with a scan rate range of 0.01–1.0 V/s. As depicted in Figure 3C,D, the redox peak currents increased gradually with the increase in the scan rate. A good linear relationship between the redox peak current ( $I_p$ ) and the square root of the scan rate ( $v^{1/2}$ ) could be achieved with the coefficient as 0.99, which indicated a diffusion-controlled electrode reaction process (Figure 3E,F). The electrochemical effective areas of the SPCE and a-GC/SPCE were further estimated according to Randles–Sevcik formula [38], with the results of 0.053  $\text{cm}^2$  and 0.208  $\text{cm}^2$ , respectively. The effective area of a-GC/SPCE was 3.92 times higher than that of SPCE, which might be related to the presence of the porous structure of a-GC with a large surface area on the electrode surface.

### 2.3. Electrochemical Behaviors of DA on a-GC/SPCE

DA is an important neurotransmitter with a hydroxyl functional group in the molecular structure, which can be electro-oxidized on the electrode surface. The electrochemical behaviors of DA on different modified electrodes were investigated in 0.1 mol/L phosphate buffered saline (PBS, pH 6.0) containing 0.5 mmol/L DA, with the results shown in Figure 4. In the voltammogram obtained at a bare SPCE (curve a), an oxidation peak of 20.89  $\mu\text{A}$  at 0.57 V ( $E_{pa}$ ) and a reduction peak of 16.76  $\mu\text{A}$  at 0.00 V ( $E_{pc}$ ) were observed, which corresponded to a peak separation ( $\Delta E_p$ ) of 0.57 V. Similarly, the CV obtained at an a-GC/SPCE (curve b) shows a  $I_{pa}$  of 37.22  $\mu\text{A}$  at 0.28 V and a  $I_{pc}$  of 33.37  $\mu\text{A}$  at 0.14 V, giving an  $\Delta E_p$  of 0.14 V. The decrease in the  $\Delta E_p$  value (from 0.57 V to 0.14 V) proved that a-GC could provide excellent conductivity and high surface areas for the redox of DA. And these results might be because that the a-GC with layered structures can effectively reduce the diffusion length of ions from the electrolyte and provide additional active area. In addition, a significant shift in the oxidation peak to the lower potential with improved peak currents was observed on a-GC/SPCE, which could also be ascribed to the electrocatalytic activity and fast electron transport efficiency of a-GC.

### 2.4. Electrochemical Investigations of DA on a-GC/SPCE

The influence of the scan rate on the cyclic voltametric response of 0.1 mmol/L DA was investigated using GC-a/SPCE in 0.1 mol/L PBS (pH 6.0) and the results are shown in Figure 5A. It can be seen that the increase in the scan rate from 0.01 V/s to 0.5 V/s led to the increase in the redox peak current. As depicted in Figure 5B, the redox peak current is directly proportional to the square root of the scan rate ( $v^{1/2}$ ), with the linear regression equations set as  $I_{pa}$  ( $\mu\text{A}$ ) = 45.4  $v^{1/2}$  (V/s) – 7.49 ( $R = 0.995$ ,  $N = 10$ ) and  $I_{pc}$  ( $\mu\text{A}$ ) = –87.2  $v^{1/2}$  (V/s) + 2.32 ( $R = 0.994$ ,  $N = 10$ ), which indicated a diffusion-control reaction process of DA on a-GC/SPCE. The relation between the  $I_{pa}$  ( $\mu\text{A}$ ) and the square root of scan rate ( $v^{1/2}$ ) is given by the Randles–Sevcik equation:  $I_{pa} = (2.69 \times 10^5) n^{3/2} A C_0 D_0^{1/2} v^{1/2}$ , where  $n$  is the number of electrons exchanged in oxidation at  $T = 298$  K,  $A$  is the effective electrode area (0.208  $\text{cm}^2$ ),  $C_0$  is the DA concentration ( $1.0 \times 10^{-4}$  mol/L),  $D_0$  is the diffusion coefficient of DA ( $7.30 \times 10^{-6}$   $\text{cm}^2/\text{s}$  [39,40]), and  $v$  is the scan rate (V/s). In this way,  $n$  is evaluated as 2.08, which implies a two-electron transfer process on the a-GC/SPCE.

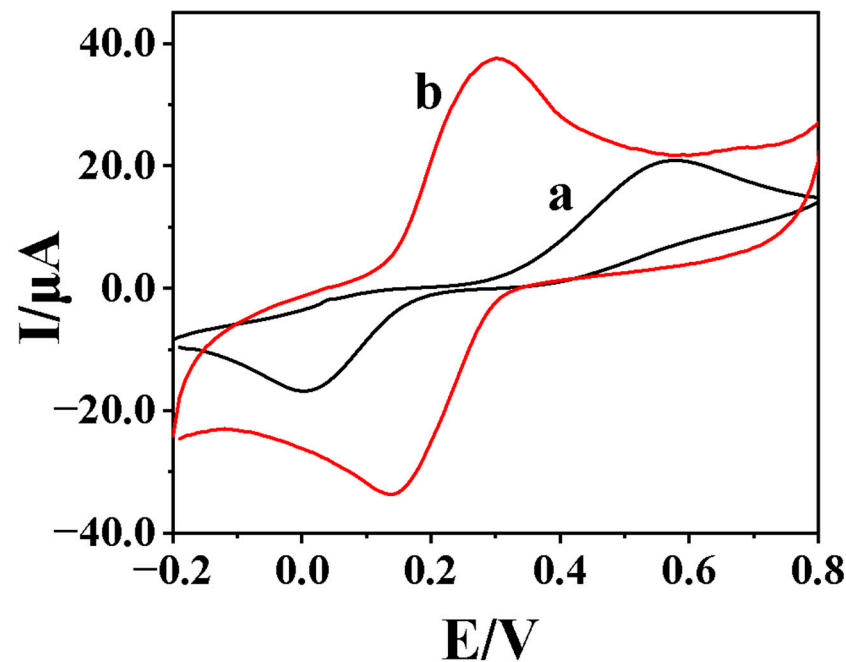


**Figure 4.** Cyclic voltammograms of 0.5 mmol/L DA on (a) SPCE and (b) a-GC/SPCE in 0.1 mol/L PBS (pH 6.0); scan rate of 0.1 V/s.

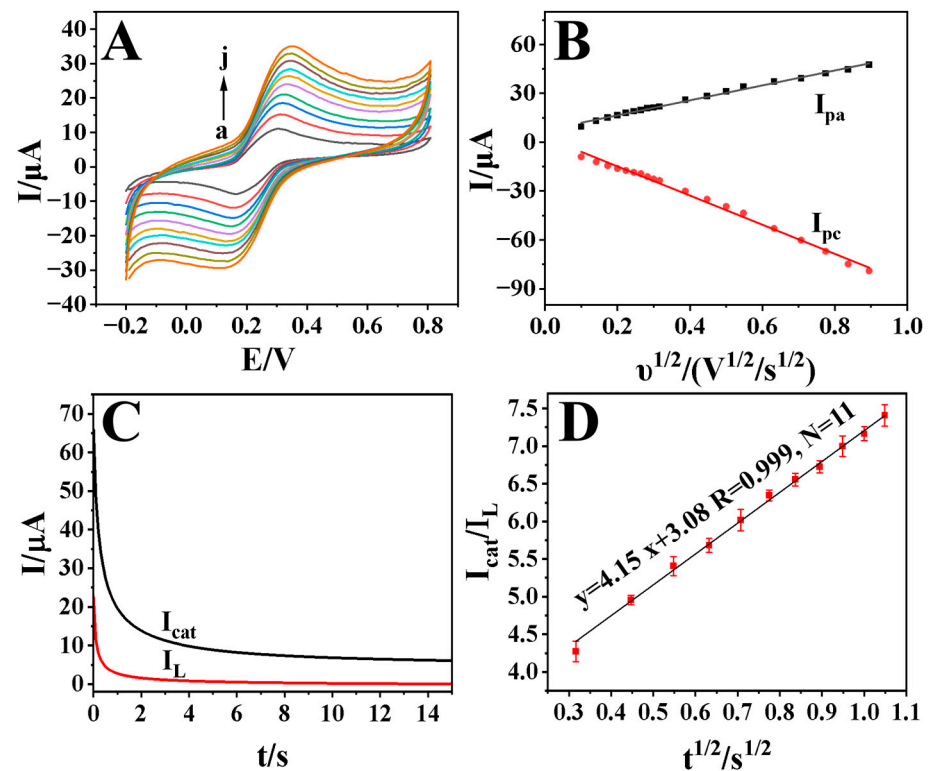


**Figure 5.** (A) Cyclic voltammograms of a-GC/SPCE at different scan rates (a–j: 0.01, 0.02, 0.03, 0.04, 0.05, 0.06, 0.07, 0.08, 0.09, 0.1, 0.15, 0.2, 0.25, 0.3, 0.35, 0.4, 0.45, 0.5 V/s) in 0.1 mmol/L DA and PBS (pH 6.0) and (B) the corresponding relationship of  $I_p$  versus  $v^{1/2}$ , (C) chronoamperometric response of a-GC/SPCE in 0.1 mol/L PBS (pH 6.0) in the absence ( $I_L$ ) and presence ( $I_{cat}$ ) of 0.1 mmol/L DA, (D) the corresponding relationship of  $I_{cat}/I_L$  versus  $t^{1/2}$ .

To further evaluate the electrocatalytic parameter and electrochemical kinetic of DA on the surface of a-GC/SPCE, the chronoamperometric responses on a-GC/SPCE were



investigated in the absence ( $I_L$ ) and presence ( $I_{cat}$ ) of 0.1 mmol/L DA solution at the potential of 0.5 V (Figure 5C). The catalytic rate constant ( $k_{cat}$ ) of DA oxidation could be obtained using the following equation [41]:  $I_{cat}/I_L = (\pi k_{cat} C_0 t)^{1/2}$ , where  $I_{cat}$  and  $I_L$  are the current on the a-GC/SPCE in the presence and absence of DA, respectively, and  $t$  is the elapsed time. From the slope of the  $I_{cat}/I_L$  vs.  $t^{1/2}$  plot (Figure 5D), the value of  $k_{cat}$  was found to be  $5.48 \times 10^4 \text{ M}^{-1} \text{ s}^{-1}$ , which was obviously larger than that reported in the literature ( $8.81 \times 10^3 \text{ M}^{-1} \text{ s}^{-1}$  [42],  $2.57 \times 10^4 \text{ M}^{-1} \text{ s}^{-1}$  [43],  $6.80 \times 10^2 \text{ M}^{-1} \text{ s}^{-1}$  [44]). The results prove that a-GC has good electrocatalytic activity for electrochemical oxidation of DA.

The influence of the pH of PBS was studied based on the CV of 0.1 mmol/L DA on a-GC/SPCE in 0.1 mol/L PBS with the pH value varying from 3.0 to 8.0. The results obtained are depicted in Figure 6A. Here, the oxidation peak of DA was observed to shift negatively from 0.35 V to 0.14 V, and the reduction peak to shift from 0.31 V to 0.09 V, with the increase in the pH from 3.0 to 7.0, indicating that protons were involved in the electrode reaction. As shown in Figure 6B, a linear relationship between the formal peak potential ( $E^{0'}$ ; estimated using the average of  $E_{pa}$  and  $E_{pc}$ ) and pH was obtained with the linear regression equation set as  $E^{0'}(\text{V}) = 0.48 - 0.054 \text{ pH}$  ( $R = 0.993$ ,  $N = 5$ ). The slope value of 54 mV/pH was close to the theoretical value of 59 mV/pH for an equal number of protons and electrons involved in the electrode reaction. The oxidation peak current increased gradually with the increase in the pH from 3.0 to 6.0, and it reached a maximum value at the pH value of 6.0 and then decreased at pH 7–8, so pH 6.0 was selected for further investigation. The decrease in the oxidation peak current at pH 7–8 was likely because DA could self-polymerize into polydopamine in neutral and alkaline solutions [45,46]. DA can be polymerized in the electrolyte under alkaline conditions, which led to the decrease in the concentration of free DA in the solution, resulting in a decrease in the redox peak current.

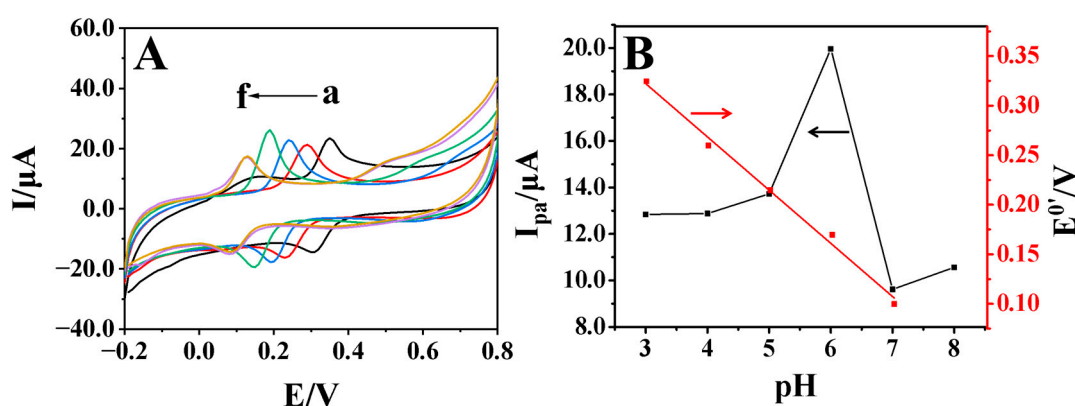
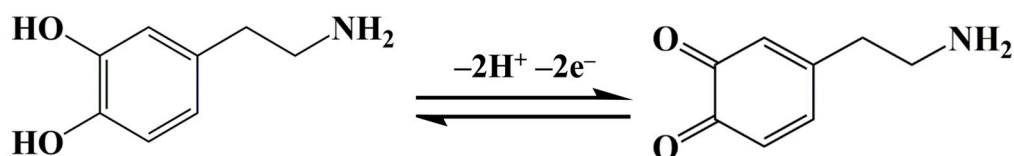


**Figure 6.** (A) Cyclic voltammograms of a-GC/SPCE in 0.1 mmol/L DA with different pH values (a→f: pH 3.0, 4.0, 5.0, 6.0, 7.0, 8.0), (B) the plot of  $I_{pa}$  (black line) and  $E^{0'}$  (red line) of DA versus pH.

As the electrooxidation process is isoelectronic and isoprotonic, DA exhibits a two electrons and two protons process on a-GC/SPCE. The oxidation mechanism is shown in Scheme 2, in which DA loses two electrons and two protons to become dopamine-o-quinone. Then, the reduction reaction occurs according to the reverse process.



**Scheme 2.** Electrochemical oxidation mechanism of DA on a-GC/SPCE.

### 2.5. Calibration Study for DA Analysis

The differential pulse voltammetry (DPV) method was used for the quantitative analysis of DA in this study. As shown in Figure 7A, the oxidation peak current increased gradually with the DA concentrations ranging from 1.0–1000.0  $\mu\text{mol/L}$ . Good linear relationships were obtained between the oxidation peak currents and DA concentration (Figure 7B) in the range from 1.0–150.0  $\mu\text{mol/L}$  and 150.0–1000.0  $\mu\text{mol/L}$ , with the linear regression equations set as  $I_1(\mu\text{A}) = 1.50 C_{\text{DA}} (\mu\text{mol/L}) + 43.2$  ( $R = 0.996$ ,  $N = 8$ ) and  $I_2(\mu\text{A}) = 0.100 C_{\text{DA}} (\mu\text{mol/L}) + 241$  ( $R = 0.995$ ,  $N = 7$ ). The sensitivity (slope) of the calibration plot decreased from 1.5  $\mu\text{A}/(\mu\text{mol/L})$  to 0.1  $\mu\text{A}/(\mu\text{mol/L})$  when the DA concentration was higher than 150.0  $\mu\text{mol/L}$ , which might be due to the active sites on the surface of a-GC/SPCE decreasing relative to the total number of DA molecules [47]. Based on a signal-to-noise ratio of 3, the limit of detection (LOD) was estimated to be 0.25  $\mu\text{mol/L}$  using the linear calibration results between 1.0 and 150.0  $\mu\text{mol/L}$ . The analytical parameters of DA using different modified electrodes and detection methods are listed in Table 1, which indicates that a-GC/SPCE has a comparable LOD and wider linear range with others. The wider linear range may be due to the large surface area and more electroactive sites of a-GC, which is conducive to the adsorption and reaction of DA molecules. In addition, a-GC/SPCE exhibits considerable merits, including low-cost raw materials and portable detection on smart phones with a small size U-disk electrochemical workstation, which is more suitable for the point-of-care testing.

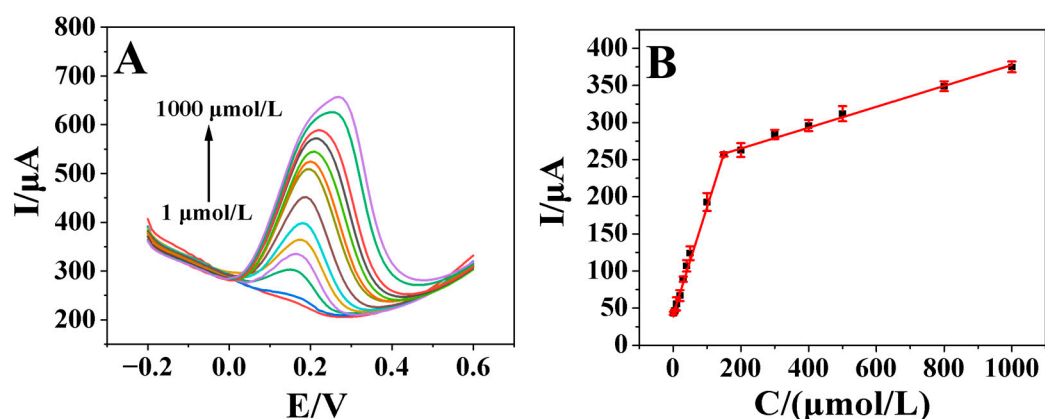


**Figure 7.** (A) Differential pulse voltammograms of a-GC/SPCE in different concentrations of DA and (B) the relationships of the oxidation peak currents with the DA concentrations.

**Table 1.** Comparison of the analytical performances of different electrochemical DA sensors.

Electrodes	Methods	Linear Range ( $\mu\text{mol/L}$ )	LOD ( $\mu\text{mol/L}$ )	References
Au@Pt/GO/GCE	DPV	1.0–100.0	5.0	[48]
CA/GCE	CV	5–100	0.86	[49]
LS-rGO/GCE	DPV	0.12–100	0.035	[50]
Pd-NPs-rGO/GCE	LSV	1–150	0.233	[51]
Graphene/GCE	DPV	4–100	2.64	[52]
Nafion/CCINPs-CS/GCE	DPV	2.0–60	1.0	[53]
N-rGO/GCE	DPV	1–60	0.1	[54]
rGS-GNP/Au	DPV	0.1–100	0.098	[55]
f-MWCNT/AgNP/GCE	DPV	1–8	0.2778	[56]
GQDs-MWCNTs/GCE	DPV	0.05–100.0	0.00087	[57]
PtAu/GCE	DPV	24–384	24	[58]
a-GC/SPCE	DPV	1.0–150.0 150.0–1000.0	0.25	This work

Note: GO: graphene oxide; GCE: glassy carbon electrode; CA: catechol; LS: lignosulfonate; rGO: reduced graphene oxide; Pd-NPs: platinum nanoparticles; CCINPs-CS: carbon-coated iron nanoparticles and chitosan composite; N-rGO: nitrogen-doped reduced graphene oxide; rGS: reduced graphene oxide sheet; GNP: gold nanoparticle; MWCNT: multi-walled carbon nanotube; GQDs: graphene quantum dots.

### 2.6. Selectivity, Repeatability and Stability

In order to investigate the selectivity of a-GC/SPCE, differential pulse voltammograms of 25.0  $\mu\text{mol/L}$  DA containing 50.0  $\mu\text{mol/L}$  common interferences (such as  $\text{Ca}^{2+}$ ,  $\text{SO}_4^{2-}$ ,  $\text{NO}_3^-$ ,  $\text{K}^+$ ,  $\text{Na}^+$ , AA, urea and UA) were recorded. As shown in Figure 8A, there was no significant influences on the oxidation currents of DA in the presence of these interferences (with the signal change of less than 6%), which proved that a-GC/SPCE had good selectivity. And the change in the current value after adding 50.0  $\mu\text{mol/L}$  common interferences were normalized to 1 and plotted in the radar graph of Figure 8A in order to visualize the selectivity of a-GC/SPCE. Multi-sweep cyclic voltammetry was used to record 50 cycles of five a-GC/SPCE. The results showed that the currents of the five electrodes were basically unchanged. After the modified electrode was stored at room temperature for 7 days, the peak current measured in 25.0  $\mu\text{mol/L}$  DA solution remained 97.56% of the initial value with the relative standard deviation (RSD) of the current less than 4.6% (Figure 8B). The above results indicated that the sensor had good selectivity, stability and reproducibility for DA analysis.

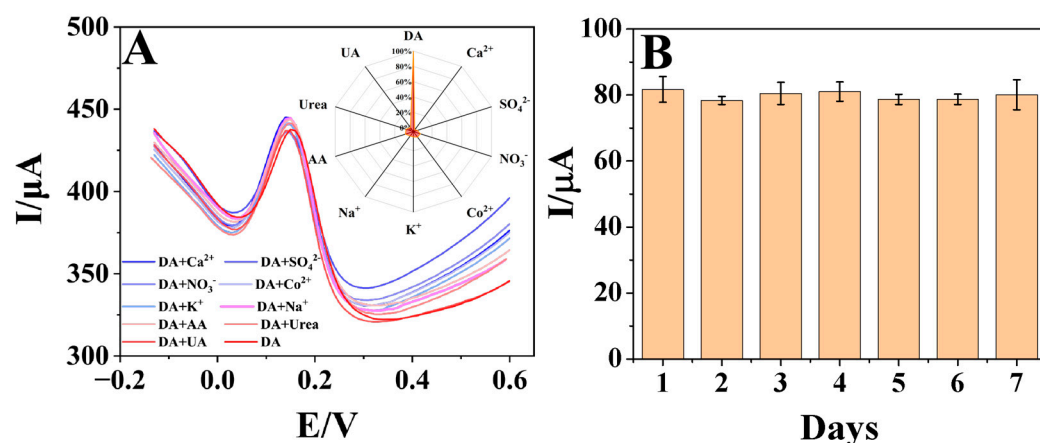


**Figure 8.** (A) Differential pulse voltammograms of a-GC/SPCE in 25.0  $\mu\text{mol/L}$  DA solution containing 50.0  $\mu\text{mol/L}$  interfering substance (inset is the corresponding selectivity), and (B) the oxidation current values of a-GC/SPCE in 25.0  $\mu\text{mol/L}$  DA for 7 days.

### 2.7. Real-Life Sample Analysis

As compared with other body fluids, sweat has advantages such as easy sampling, simplicity of operation and obtainment; thus, human sweat was used as the real-life sample to explore the reliability of a-GC/SPCE. The sweat sample was diluted 10 times with 0.1 mol/L PBS (pH 6.0) and a standard addition calibration method was performed to estimate the DA concentration. After three parallel experiments were conducted to detect the concentration of DA, the results obtained through calibration are listed in Table 2. The recovery was 98.90~102.30% via the standard addition method with a calculated RSD value less than 3.0%. Therefore, a-GC/SPCE has potential application prospects in the actual detection of DA.

**Table 2.** Detection results of DA in human sweat samples.

Samples	Added ( $\mu\text{mol/L}$ )	Found ( $\mu\text{mol/L}$ )	Recovery (%)	RSD (%)
Human sweat	10.00	10.23	102.30	2.48
	20.00	19.78	98.90	1.43
	30.00	29.76	99.20	2.29

### 3. Experimental

#### 3.1. Instruments and Reagents

Dopamine (DA > 98%) were obtained from Shanghai Aladdin Reagent Co., Ltd., (Shanghai, China). Tilapia fish scales were acquired from local supermarkets. Potassium ferricyanide ( $K_3[Fe(CN)_6]$ ) were purchased from Guangzhou Chemical Reagent Factory (Guangzhou, China). Sweat samples were collected from volunteers' faces following vigorous exercise using 1.5 mL centrifuge tubes. These samples were then filtered using a 0.22  $\mu\text{m}$  syringe filter before being stored at 4 °C for further examination. In our work, 0.1 mol/L PBS (pH 6.0) was used as a supporting electrolyte. All the reagents were of analytical grade and all the solutions were prepared with ultrapure water (specific resistance of 18  $M\Omega\text{-cm}$ ) obtained from a Milli-Q Plus system (Millipore, IQ7000, Merck Millipore Co., Ltd., Burlington, MA, USA).

Electrochemical experiments were conducted using a U-disk electrochemical workstation (Sensit Smart U disk, Palmsens Co., Ltd., Houten, The Netherlands), which was connected and controlled via a Huawei smart phone with Bluetooth. The SPCE is integrated with a three-electrode system comprising a carbon ink-printed electrode (5.0 mm diameter) as a working electrode, an Ag/AgCl reference electrode, and a carbon counter electrode, which was provided by Weihai Potential Technology Co., Ltd. (Weihai, China). The morphologies and elemental analysis of a-GC were recorded via SEM (Apreo SEM, Thermo Fisher Scientific, Trondheim, Norway) coupled with EDS (X-Max, Oxford instruments, Abingdon, UK), and the microstructures were characterized using field emission TEM (JEM-2100F, Japan Electronics Co., Ltd., Tokyo, Japan). XRD (X-pert 3, PANalytical B.V., Almelo, The Netherlands) was applied to study the crystal phase structure of a-GC with a  $\text{Cu K}\alpha$  radiation at wavelength of 1.5406 Å. The Raman spectrum in the range from 500 to 3500  $\text{cm}^{-1}$  was obtained on a LabRAM HR system using a 532 nm laser (Horiba, Palaiseau, France). The  $\text{N}_2$  adsorption and desorption isotherms, surface area and pore size distribution of a-GC were studied on a Physical Adsorption Instrument (ASAP 2020, Micromeritics Co., Phoenix, AZ, USA).

#### 3.2. Synthesis of a-GC

The carbon precursor was prepared using an enzymatic hydrolysis method previously reported by our group [27]. Briefly, tilapia fish scales were sequentially soaked in a concentration of HCl and 10 wt% NaOH to remove inorganic salts and hydroxyapatite. Then, 12.5 g of the treated product was added to a 250 mL aqueous solution containing 3.0 g alkaline protease, and then stirred at 75 °C for 12 h. The product was filtered using a 0.45  $\mu\text{m}$  and a 0.2  $\mu\text{m}$  filter membrane, and heated at 75 °C for 4 h with magnetic stirring to obtain a homogeneous concentrated carbon precursor solution.

Next, 0.33 g  $K_3[Fe(CN)_6]$  was dissolved homogeneously in 30 mL precursor and further heated until the solvent was completely evaporated. The dried solid was transferred to a tube furnace and carbonized in  $\text{N}_2$  at 1000 °C for 2 h, with a heating rate of 5 °C /min. The obtained sample was washed with ultrapure water several times and dried in a vacuum at 100 °C for 12 h to obtain GC-Fe. The GC-Fe was soaked in 36 wt% HCl for 24 h at room temperature to remove iron, then the solid was washed with ultrapure water several times to a neutral pH, and dried at 80 °C overnight to obtain the black solid named GC.

The alkaline activation treatment was performed with the following procedure. GC and KOH were mixed evenly at a mass ratio of 1:4, and the mixture was held in an 800 °C tube furnace with an  $\text{N}_2$  atmosphere for 1 h. Finally, the product was washed with ultrapure water to neutrality, and then dried at 60 °C overnight to obtain alkali-activated graphite carbon, which was denoted as a-GC.

#### 3.3. Electrochemical Investigations

In our work, 1.5 mg/mL a-GC suspension was prepared in ultrapure water. Then, 25  $\mu\text{L}$  of the above suspension was applied to the SPCE surface and dried at room temperature to obtain a-GC/SPCE. The electrochemical behaviors of DA on different modified

electrodes were studied by means of CV, DPV and chronoamperometry using a U-disk workstation connected with a smart phone with Bluetooth and Android system. The CV parameters were set in the potential range of  $-0.2\sim 0.8$  V, with the scan speed set as 0.1 V/s. DPV was carried out with the following parameters: potential range from  $-0.2$  to 0.6 V, pulse width of 50 ms, pulse increment of 10 mV, pulse amplitude of 50 mV. Chronoamperometry was measured at an initial potential of 0.2 V, interval time of 0.1 s and run time of 15 s.

#### 4. Conclusions

In this paper, fish scales were handled with enzymolysis, carbonization and activation to synthesize the a-GC. The electrochemical characterizations showed that the a-GC derived from fish scales can act as an excellent modifier for electrochemical sensors. In addition, activation and graphitization have effectively improved the porosity and graphitization degree of biomass carbon, which was demonstrated to enhance the electrochemical performances of the modified electrode. The a-GC-modified SPCE was further used to construct a portable electrochemical sensor for DA detection by combining it with the U-disk electrochemical workstation and a smart phone with two linear ranges of 1.0–150.0  $\mu\text{mol/L}$  and 150.0–1000.0  $\mu\text{mol/L}$ . Based on a signal-to-noise ratio of 3, a limit of detection of 0.25  $\mu\text{mol/L}$  was estimated. The proposed method was successfully applied to the quantitative detection of human sweat samples, with satisfactory results, which provided an opportunity for developing noninvasive diagnosis and nursing equipment of DA.

**Author Contributions:** F.Y.: writing—original draft, methodology and data curation. X.H.: writing—original draft, methodology and data curation. Y.A.: data curation and conceptualization. B.S.: investigation and software. W.D.: formal analysis and supervision. K.T.: conceptualization and validation. W.S.: project administration and funding acquisition. All authors have read and agreed to the published version of the manuscript.

**Funding:** This work was supported by the China Geological Survey Project “Wetland Resources Survey of International Importance in South China” (No. DD20220876), Survey and Evaluation of Strategic Mineral Resources in Key Sea Areas of Eastern Hainan Island.

**Institutional Review Board Statement:** Not applicable.

**Informed Consent Statement:** Not applicable.

**Data Availability Statement:** Data are contained within the article.

**Conflicts of Interest:** The authors declare no conflicts of interest.

#### References

1. Kelley, A.E. Memory and addiction: Shared neural circuitry and molecular mechanisms. *Neuron* **2004**, *44*, 161–179. [[CrossRef](#)] [[PubMed](#)]
2. Caudle, W.M.; Colebrooke, R.E.; Emson, P.C.; Miller, G.W. Altered vesicular dopamine storage in Parkinson’s disease: A premature demise. *Trends Neurosci.* **2008**, *31*, 303–308. [[CrossRef](#)]
3. Brunmair, J.; Gotsmy, M.; Niederstaetter, L.; Neuditschko, B.; Bileck, A.; Slany, A.; Feuerstein, M.L.; Langbauer, C.; Janker, L.; Zanghellini, J.; et al. Finger sweat analysis enables short interval metabolic biomonitoring in humans. *Nat. Commun.* **2021**, *12*, 5993. [[CrossRef](#)] [[PubMed](#)]
4. Baker, L.B.; Wolfe, A.S. Physiological mechanisms determining eccrine sweat composition. *Eur. J. Appl. Physiol.* **2020**, *120*, 719–752. [[CrossRef](#)] [[PubMed](#)]
5. Bariya, M.; Nyein, H.Y.Y.; Javey, A. Wearable sweat sensors. *Nat. Electron.* **2018**, *1*, 160–171. [[CrossRef](#)]
6. Wei, X.; Zhang, Z.D.; Wang, Z.H. A simple dopamine detection method based on fluorescence analysis and dopamine polymerization. *Microchem. J.* **2019**, *145*, 55–58. [[CrossRef](#)]
7. Tang, H.; Lin, P.; Chan, H.L.; Yan, F. Highly sensitive dopamine biosensors based on organic electrochemical transistors. *Biosens. Bioelectron.* **2011**, *26*, 4559–4563. [[CrossRef](#)]
8. Jiang, Z.; Gao, P.; Yang, L.; Huang, C.; Li, Y. Facile in situ synthesis of silver nanoparticles on the surface of metal–organic framework for ultrasensitive surface-enhanced Raman scattering detection of dopamine. *Anal. Chem.* **2015**, *87*, 12177–12182. [[CrossRef](#)] [[PubMed](#)]

9. Chen, A.C.; Chatterjee, S. Nanomaterials based electrochemical sensors for biomedical applications. *Chem. Soc. Rev.* **2013**, *42*, 5425–5438. [[CrossRef](#)]
10. Wilson, D.M.; Hoyt, S.; Janata, J.; Booksh, K.; Obando, L. Chemical sensors for portable, handheld field instruments. *IEEE Sens. J.* **2001**, *4*, 256–274. [[CrossRef](#)]
11. Shao, B.; Ai, Y.J.; Yan, L.J.; Wang, B.L.; Huang, Y.H.; Zou, Q.W.; Fu, H.Y.; Niu, X.L.; Sun, W. Wireless electrochemical sensor for the detection of phytohormone indole-3-acetic acid using gold nanoparticles and three-dimensional reduced graphene oxide modified screen printed carbon electrode. *Talanta* **2023**, *253*, 124030. [[CrossRef](#)]
12. Parrilla, M.; Montiel, N.F.; Van Durme, F.; De Wael, K. Derivatization of amphetamine to allow its electrochemical detection in illicit drug seizures. *Sens. Actuat. B Chem.* **2021**, *337*, 129819. [[CrossRef](#)]
13. Chen, Y.X.; Sun, Y.X.; Niu, Y.Y.; Wang, B.L.; Zhang, Z.J.; Zeng, L.N.; Li, L.; Sun, W. Portable electrochemical sensing of indole-3-acetic acid based on self-assembled MXene and multi-walled carbon nanotubes composite modified screen-printed electrode. *Electroanalysis* **2023**, *35*, e202200279. [[CrossRef](#)]
14. Zhou, J.H.; Pan, K.H.; Qu, G.F.; Ji, W.; Ning, P.; Tang, H.M.; Xie, R.S. rGO/MWCNTs-COOH 3D hybrid network as a high-performance electrochemical sensing platform of screen-printed carbon electrodes with an ultra-wide detection range of Cd (II) and Pb (II). *Chem. Eng. J.* **2022**, *449*, 137853. [[CrossRef](#)]
15. Yamuna, A.; Karikalan, N.; Na, J.H.; Lee, T.Y. Lanthanum tin oxide-modified sensor electrode for the rapid detection of environmentally hazardous insecticide carbaryl in soil, water, and vegetable samples. *J. Hazard. Mater.* **2022**, *437*, 129415. [[CrossRef](#)] [[PubMed](#)]
16. Nagles, E.; García-Beltrán, O.; Calderón, J.A. Evaluation of the usefulness of a novel electrochemical sensor in detecting uric acid and dopamine in the presence of ascorbic acid using a screen-printed carbon electrode modified with single walled carbon nanotubes and ionic liquids. *Electrochim. Acta* **2017**, *258*, 512–523. [[CrossRef](#)]
17. Palanisamy, S.; Thirumalraj, B.; Chen, S.M.; Ali, M.A.; Al-Hemaid, F.M. Palladium nanoparticles decorated on activated fullerene modified screen printed carbon electrode for enhanced electrochemical sensing of dopamine. *J. Colloid. Interf. Sci.* **2015**, *448*, 251–256. [[CrossRef](#)] [[PubMed](#)]
18. Dakshayini, B.S.; Reddy, K.R.; Mishra, A.; Shetti, N.P.; Malode, S.J.; Basu, S.; Naveen, S.; Raghu, A.V. Role of conducting polymer and metal oxide-based hybrids for applications in amperometric sensors and biosensors. *Microchem. J.* **2019**, *147*, 7–24. [[CrossRef](#)]
19. Li, Z.; Wang, L.; Li, Y.; Feng, Y.; Feng, W. Carbon-based functional nanomaterials: Preparation, properties and applications. *Compos. Sci. Technol.* **2019**, *179*, 10–40. [[CrossRef](#)]
20. Islam, S.; Shaheen Shah, S.; Naher, S.; Ali Ehsan, M.; Aziz, M.A.; Ahammad, A.S. Graphene and carbon nanotube-based electrochemical sensing platforms for dopamine. *Chem. Asian J.* **2021**, *16*, 3516–3543. [[CrossRef](#)] [[PubMed](#)]
21. Wang, W.; Xu, G.; Cui, X.T.; Sheng, G.; Luo, X. Enhanced catalytic and dopamine sensing properties of electrochemically reduced conducting polymer nanocomposite doped with pure graphene oxide. *Biosens. Bioelectron.* **2014**, *58*, 153–156. [[CrossRef](#)]
22. Manasa, P.; Sambasivam, S.; Ran, F. Recent progress on biomass waste derived activated carbon electrode materials for supercapacitors applications—A review. *J. Energy Storage* **2022**, *54*, 105290. [[CrossRef](#)]
23. Zhang, W.; Liu, L.; Li, Y.; Wang, D.; Ma, H.; Ren, H.; Shi, Y.; Han, Y.; Ye, B.C. Electrochemical sensing platform based on the biomass-derived microporous carbons for simultaneous determination of ascorbic acid, dopamine, and uric acid. *Biosens. Bioelectron.* **2018**, *121*, 96–103. [[CrossRef](#)] [[PubMed](#)]
24. Mahmood, F.; Sun, Y.; Wan, C. Biomass-derived porous graphene for electrochemical sensing of dopamine. *RSC Adv.* **2021**, *11*, 15410–15415. [[CrossRef](#)] [[PubMed](#)]
25. Padmapriya, A.; Thiagarajan, P.; Devendiran, M.; Kalaivani, R.A.; Shanmugharaj, A.M. Electrochemical sensor based on N, P-doped carbon quantum dots derived from the banana flower bract (*Musa acuminata*) biomass extract for selective and picomolar detection of dopamine. *J. Electroanal. Chem.* **2023**, *943*, 117609. [[CrossRef](#)]
26. Sha, T.; Li, X.; Liu, J.; Sun, M.; Wang, N.; Bo, X.; Guo, Y.; Hu, Z.; Zhou, M. Biomass waste derived carbon nanoballs aggregation networks-based aerogels as electrode material for electrochemical sensing. *Sens. Actuat. B Chem.* **2018**, *277*, 195–204. [[CrossRef](#)]
27. Wang, B.; Shi, F.; Sun, Y.; Yan, L.; Zhang, X.; Wang, B.; Sun, W. Ni-enhanced molybdenum carbide loaded N-doped graphitized carbon as bifunctional electrocatalyst for overall water splitting. *Appl. Surf. Sci.* **2022**, *572*, 151480. [[CrossRef](#)]
28. Lu, Q.; Ye, X.N.; Zhang, Z.X.; Wang, Z.X.; Cui, M.S.; Yang, Y.P. Catalytic fast pyrolysis of sugarcane bagasse using activated carbon catalyst in a hydrogen atmosphere to selectively produce 4-ethyl phenol. *J. Anal. Appl. Pyrolysis* **2018**, *136*, 125–131. [[CrossRef](#)]
29. Shi, F.; Yan, L.J.; Li, X.Q.; Feng, C.L.; Wang, C.Z.; Zhang, B.X.; Sun, W. Porous biomass carbon and gold nanoparticles modified electrode for myoglobin direct electrochemistry and electrocatalysis. *J. Chin. Chem. Soc.* **2021**, *68*, 2006–2012. [[CrossRef](#)]
30. Ai, Y.; Liu, J.; Yan, L.; Li, G.; Wang, X.; Sun, W. Banana peel derived biomass carbon: Multi-walled carbon nanotube composite modified electrode for sensitive voltammetric detection of baicalein. *J. Chin. Chem. Soc.* **2022**, *69*, 359–365. [[CrossRef](#)]
31. Balahmar, N.; Al-Jumaily, A.S.; Mokaya, R. Biomass to porous carbon in one step: Directly activated biomass for high performance CO<sub>2</sub> storage. *J. Mater. Chem. A* **2017**, *5*, 12330–12339. [[CrossRef](#)]
32. He, H.; Zhang, R.; Zhang, P.; Wang, P.; Chen, N.; Qian, B.; Zhang, L.; Yu, J.; Dai, B. Functional carbon from nature: Biomass-derived carbon materials and the recent progress of their applications. *Adv. Sci.* **2023**, *10*, 2205557. [[CrossRef](#)] [[PubMed](#)]
33. Cheng, D.; Tian, M.; Wang, B.; Zhang, J.; Chen, J.; Feng, X.; He, Z.; Dai, L.; Wang, L. One-step activation of high-graphitization N-doped porous biomass carbon as advanced catalyst for vanadium redox flow battery. *J. Colloid. Interf. Sci.* **2020**, *572*, 216–226. [[CrossRef](#)]

34. He, J.; Zhang, D.; Wang, Y.; Zhang, J.; Yang, B.; Shi, H.; Wang, K.; Wang, Y. Biomass-derived porous carbons with tailored graphitization degree and pore size distribution for supercapacitors with ultra-high rate capability. *Appl. Surf. Sci.* **2020**, *515*, 146020. [CrossRef]
35. Zhao, J.; Liu, Y.; Quan, X.; Chen, S.; Yu, H.; Zhao, H. Nitrogen-doped carbon with a high degree of graphitization derived from biomass as high-performance electrocatalyst for oxygen reduction reaction. *Appl. Surf. Sci.* **2017**, *396*, 986–993. [CrossRef]
36. Adekunle, A.S.; Agboola, B.O.; Pillay, J.; Ozoemena, K.I. Electrocatalytic detection of dopamine at single-walled carbon nanotubes–iron (III) oxide nanoparticles platform. *Sens. Actuat. B Chem.* **2010**, *148*, 93–102. [CrossRef]
37. Ferrari, A.C.; Meyer, J.C.; Scardaci, V.; Casiraghi, C.; Lazzeri, M.; Mauri, F.; Piscanec, S.; Jiang, D.; Novoselov, K.S.; Roth, S.; et al. Raman spectrum of graphene and graphene layers. *Phys. Rev. Lett.* **2006**, *97*, 187401. [CrossRef]
38. Bard, A.J.; Faulkner, L.R.; White, H.S. *Electrochemical Methods: Fundamentals and Applications*; John Wiley Sons: Hoboken, NJ, USA, 1983; Volume 60, p. A25. [CrossRef]
39. Ensafi, A.A.; Taei, M.; Khayamian, T.; Arabzadeh, A. Highly selective determination of ascorbic acid, dopamine, and uric acid by differential pulse voltammetry using poly (sulfonazo III) modified glassy carbon electrode. *Sens. Actuat. B Chem.* **2010**, *147*, 213–221. [CrossRef]
40. Mazloum Ardakani, M.; Beitollahi, H.; Ganjipour, B.; Naeimi, H.; Nejati, M. Electrochemical and catalytic investigations of dopamine and uric acid by modified carbon nanotube paste electrode. *Bioelectrochemistry* **2009**, *75*, 1–8. [CrossRef]
41. Galus, Z. *Fundamentals of Electrochemical Analysis*; Ellis Horwood: New York, NY, USA, 1976; Volume 10. Available online: <https://lcn.loc.gov/76005838> (accessed on 28 January 2024).
42. Xu, Y.; Qin, Y.; Gao, X.; Li, J.; Xiao, D. Defective prussian blue analogue with cobalt for fabrication of an electrochemical sensor for detecting ascorbic acid, dopamine and uric acid. *Chem. Electro. Chem.* **2023**, *10*, e202300134. [CrossRef]
43. Zhang, W.; Zheng, J.; Shi, J.; Lin, Z.; Huang, Q.; Zhang, H.; Wei, C.; Chen, J.; Hu, S.; Hao, A. Nafion covered core–shell structured Fe<sub>3</sub>O<sub>4</sub>@graphene nanospheres modified electrode for highly selective detection of dopamine. *Anal. Chim. Acta* **2015**, *853*, 285–290. [CrossRef] [PubMed]
44. Gao, F.; Cai, X.; Wang, X.; Gao, C.; Liu, S.; Gao, F.; Wang, Q. Highly sensitive and selective detection of dopamine in the presence of ascorbic acid at graphene oxide modified electrode. *Sens. Actuat. B Chem.* **2013**, *186*, 380–387. [CrossRef]
45. Wei, Q.; Zhang, F.L.; Li, J.; Li, B.J.; Zhao, C.S. Oxidant-induced dopamine polymerization for multifunctional coatings. *Polym. Chem.* **2010**, *1*, 1430–1433. [CrossRef]
46. Du, X.; Li, L.X.; Li, J.S.; Yang, C.W.; Frenkel, N.; Welle, A.; Heissler, S.; Nefedov, A.; Grunze, M.; Levkin, P.A. UV-triggered dopamine polymerization: Control of polymerization, surface coating, and photopatterning. *Adv. Mater.* **2014**, *26*, 8029–8033. [CrossRef] [PubMed]
47. Molaakbari, E.; Mostafavi, A.; Beitollahi, H. Simultaneous electrochemical determination of dopamine, melatonin, methionine and caffeine. *Sens. Actuat. B Chem.* **2015**, *208*, 195–203. [CrossRef]
48. Yang, Z.; Liu, X.; Zheng, X.; Zheng, J. Synthesis of Au@Pt nanoflowers supported on graphene oxide for enhanced electrochemical sensing of dopamine. *J. Electroanal. Chem.* **2018**, *817*, 48–54. [CrossRef]
49. Pourghobadi, Z.; Neamatollahi, D. Voltammetric determination of dopamine using modified glassy carbon electrode by electrografting of catechol. *J. Serb. Chem. Soc.* **2017**, *82*, 1053–1061. [CrossRef]
50. Yuan, Y.; Wang, S.; Wu, P.; Yuan, T.; Wang, X. Lignosulfonate in situ-modified reduced graphene oxide biosensors for the electrochemical detection of dopamine. *RSC Adv.* **2022**, *12*, 31083–31090. [CrossRef]
51. Palanisamy, S.; Ku, S.; Chen, S. Dopamine sensor based on a glassy carbon electrode modified with a reduced graphene oxide and palladium nanoparticles composite. *Microchim. Acta* **2013**, *180*, 1037–1042. [CrossRef]
52. Kim, Y.R.; Bong, S.; Kang, Y.J.; Yang, Y.; Mahajan, R.K.; Kim, J.S.; Kim, H. Electrochemical detection of dopamine in the presence of ascorbic acid using graphene modified electrodes. *Biosens Bioelectron.* **2010**, *25*, 2366–2369. [CrossRef] [PubMed]
53. Lai, G.S.; Zhang, H.L.; Han, D.Y. Electrocatalytic oxidation and voltammetric determination of dopamine at a Nafion/carbon-coated iron nanoparticles-chitosan composite film modified electrode. *Microchim. Acta* **2008**, *160*, 233. [CrossRef]
54. Zhang, H.; Liu, S. Electrochemical sensors based on nitrogen-doped reduced graphene oxide for the simultaneous detection of ascorbic acid, dopamine and uric acid. *J. Alloys Compd.* **2020**, *842*, 155873. [CrossRef]
55. Park, D.J.; Choi, J.H.; Lee, W.J.; Um, S.H.; Oh, B.K. Selective electrochemical detection of dopamine using reduced graphene oxide sheets-gold nanoparticles modified electrode. *J. Nanosci. Nanotechnol.* **2017**, *17*, 8012–8018. [CrossRef]
56. Anshori, I.; Nuraviana Rizalputri, L.; Rona Althof, R.; Sean Surjadi, S.; Harimurti, S.; Gumilar, G.; Yulianto, B.; Handayani, M. Functionalized multi-walled carbon nanotube/silver nanoparticle (f-MWCNT/AgNP) nanocomposites as non-enzymatic electrochemical biosensors for dopamine detection. *Nanocomposite* **2021**, *7*, 97–108. [CrossRef]
57. Huang, Q.; Lin, X.; Tong, L.; Tong, Q.X. Graphene quantum dots/multiwalled carbon nanotubes composite-based electrochemical sensor for detecting dopamine release from living cells. *ACS Sustain. Chem. Eng.* **2020**, *8*, 1644–1650. [CrossRef]
58. Thiagarajan, S.; Chen, S.M. Preparation and characterization of PtAu hybrid film modified electrodes and their use in simultaneous determination of dopamine, ascorbic acid and uric acid. *Talanta* **2007**, *74*, 212–222. [CrossRef] [PubMed]

**Disclaimer/Publisher’s Note:** The statements, opinions and data contained in all publications are solely those of the individual author(s) and contributor(s) and not of MDPI and/or the editor(s). MDPI and/or the editor(s) disclaim responsibility for any injury to people or property resulting from any ideas, methods, instructions or products referred to in the content.